Applied Physics Letters

RESEARCH ARTICLE | JULY 20 2026

Interfacial ordering reverses the boiling curve in supercritical fluids

Guohan Wu ; Xiongjiang Yu ; Jinliang Xu ; Bo Zhang

Check for updates

Appl. Phys. Lett. 129, 032701 (2026)
https://doi.org/10.1063/5.0340076

View Online Export Citation

Articles You May Be Interested In

Pool boiling inversion through bubble induced macroconvection

Appl. Phys. Lett. (March 2017)

Interplay between developing flow length and bubble departure diameter during macroconvection enhanced pool boiling

Appl. Phys. Lett. (February 2018)

Quantitative characterization of the pseudo-boiling contribution to supercritical heat transfer

Physics of Fluids (January 2024)

14 October 2026 07:12:26



AIP Publishing

Applied Physics Letters ARTICLE pubs.aip.org/aip/apl

Interfacial ordering reverses the boiling curve in supercritical fluids

Cite as: Appl. Phys. Lett. **129**, 032701 (2026); doi: 10.1063/5.0340076
Submitted: 22 April 2026 · Accepted: 2 July 2026 ·
Published Online: 20 July 2026

View Online Export Citation CrossMark

Guohan Wu, Xiongjiang Yu,[a] Jinliang Xu, and Bo Zhang

AFFILIATIONS

Beijing Key Laboratory of Multiphase Flow and Heat Transfer for Low Grade Energy Utilization, North China Electric Power University, Beijing 102206, China

[a]Author to whom correspondence should be addressed: yuxiongjiang@ncepu.edu.cn

ABSTRACT

Heat transfer in supercritical fluids is commonly interpreted as single-phase convection, where heat fluxes vary monotonically with wall superheat. In this work, a counterintuitive phenomenon, i.e., the heat fluxes increase with decreasing wall temperatures, usually termed "boiling curve reversion" in subcritical conditions, is observed on a heated wire in a supercritical fluid. Our measurements reveal that the inversion is governed by the periodic formation, lateral chain-like diffusion, and collapse of vapor-like column clusters near the heated wall. These structures separate vapor-like (VL) and liquid-like (LL) pathways and drive ordered sweeping of low-temperature, high-density fluid toward the heated surface, thereby enhancing transient heat transfer. To quantify this process, an ordered cooling intensity S is defined from the total VL–LL interfacial area and is found to correlate negatively with wall temperature. A chain-diffusion model further indicates that zero-surface-tension interfacial instability underlies the evolution of the column clusters and the resulting heat-transfer enhancement. The above results support the conclusion that self-organized interfacial ordering underlies heat-transfer-curve inversion in supercritical fluids. Our findings offer clear evidence for the two-phase nature of supercritical fluids in terms of heat transfer, providing a new framework for understanding the negative "boiling curve" in fluids with vanishing surface tension.

Published under an exclusive license by AIP Publishing. https://doi.org/10.1063/5.0340076

14 October 2026 07:12:26

Due to their exceptional thermophysical properties, supercritical fluids are of great interest in advanced energy systems, chemical processes, and thermal management under high-heat-flux conditions.[1] However, the microscopic mechanisms governing heat transfer in supercritical fluids (SFs) remain poorly understood. Conventional views typically treat supercritical heat transfer as a single-phase convection process.[2] Near the critical point, however, fluid properties vary drastically,[3] and the fluid in the near-wall region may exhibit pronounced density heterogeneity.[4] In particular, when crossing the Widom line, the fluid undergoes a continuous transition from liquid-like to vapor-like behavior.[5] This process shows certain similarities to the phase-transition behavior observed in subcritical boiling in terms of thermal response and structural reorganization.[6,7] On this basis, concepts such as the Widom line, the pseudo-critical region, and pseudo-boiling have been used to characterize the rapid structural evolution of SFs over a narrow temperature range.[8–10] Existing studies suggest that this evolution not only changes the fluid temperature but may also be accompanied by local density rearrangement and redistribution of energy, thereby giving rise to anomalous heat-transfer behavior distinct from that of conventional single-phase heat transfer. He *et al.*[11] reported bubble-like structures induced by heated-wire oscillation under conditions where the temperature was below the critical temperature, whereas the pressure exceeded the critical pressure. Nevertheless, experimental understanding of the spatial distribution of liquid-like (LL) and vapor-like (VL) structures in the near-wall region, and their relationship with wall heat transfer, remains limited.[12]

In pool heat transfer experiments with supercritical carbon dioxide (sCO_2), an anomalous phenomenon was observed: within a certain heat flux range, the wall superheat (ΔT_w) decreased rather than increased with increasing heat flux (q). Similar behavior is commonly termed *boiling inversion* in subcritical boiling.[13] Existing studies suggest that the underlying mechanisms can be broadly classified into two categories (supplementary material, S1):[14] One is associated with the extensive activation of submicrometer cavities or delayed nucleation sites at high heat flux,[15] which causes nonlinear enhancement of the heat transfer coefficient (h) and thus reduces wall superheat. The other is associated with the formation of separate liquid–vapor pathways, through which bubble-induced macroconvection or impinging liquid jets significantly enhance liquid replenishment and heat transfer,[16] thereby maintaining a relatively low wall temperature under high heat flux. However, these interpretations have been established

Published under an exclusive license by AIP Publishing

mainly for subcritical two-phase systems. Whether analogous organized fluid motions exist under supercritical conditions, and how they lead to inversion of the heat-transfer curve, still lack direct evidence and clear explanation.

To address these issues, the present study systematically investigates the inversion of sCO_2 heat transfer curves and the evolution of interfacial characteristics in a pool heat transfer system using nickel-chromium (NiCr) wires as heating elements. The wire had a diameter of 66.31 μm and an effective heating length of 26.67 mm. High-temporal-resolution, *in situ* synchronized photothermal measurements and flow visualization were performed to correlate the transient wall temperature with the evolution of near-wall VL–LL structures (supplementary material, S2). The observed enhancement shares with subcritical macroconvection the common consequence of cold fluid replenishment toward the heated surface. The distinction lies in the pathway-formation mechanism: in the present supercritical system, the ordered VL–LL pathways emerge spontaneously without deliberately engineered surface structures under vanishing surface tension. To characterize this process, an *ordered cooling intensity* (S) is further introduced, and a chain diffusion model is developed to reveal the self-organized regulatory role of VL column structures in cold fluid transport and sweeping behavior. This study provides new experimental evidence for understanding non-uniform fluid behavior in supercritical heat transfer and offers a new physical perspective on heat transfer enhancement under extreme thermal conditions.

The critical pressure and critical temperature of CO_2 are $P_c = 7.377$ MPa and $T_c = 30.98$ °C, respectively. In the present experiment, the system pressure was maintained at 8 MPa, and the bulk fluid temperature was 32.2 °C, indicating that CO_2 was in a supercritical state. As shown in Fig. 1(a), the heat transfer curve of sCO_2 at 8 MPa and 32.2 °C exhibits a pronounced reversal when ΔT_w is between 100 and 150 °C. In contrast, no such inversion is observed for CO_2 at 8 MPa and 15 °C,[11] where only the pressure exceeds the critical value. This difference is likely associated with the abrupt variation in interfacial behavior near the pseudo-critical region of sCO_2. In addition, the literature survey in Fig. 1(b) indicates that previous studies on heat transfer curve inversion have been confined mainly to subcritical conditions,[17–20] whereas the corresponding phenomenon under supercritical conditions has remained unexplored. The present analysis of pseudo-boiling inversion under supercritical conditions further deepens the understanding of the physical nature of SFs in flow and heat transfer processes. Additional measurements at 12 MPa further indicate that the inversion behavior and the associated interfacial activity are not restricted to the near-critical pressure of 8 MPa (supplementary material, S4).

Based on the *in situ* synchronized optical and thermal measurements (Fig. 2), it is observed that the heat transfer coefficient between the heated wire and the bulk fluid fluctuates in response to the formation and collapse of VL columns within the VL film covering the wire surface. The evolution process is described as follows.

During the development of the VL columns from their initial appearance to an ordered cluster, the wire surface is first fully covered by a uniform VL film at 1.43 s. Subsequently, VL columns begin to emerge in localized regions. At this stage, only a few columns appear within the field of view, and their axial lengths remain short. Meanwhile, a small dark protrusion is observed beneath the wire surface between two adjacent VL columns at 1.73 s. As time proceeds, the VL columns extend axially along the wire toward both sides; their number gradually increases, and their lengths grow significantly, while the black protrusions beneath the heated surface become more pronounced at 1.93 s. Between 1.93 and 2.78 s, the VL columns continue to expand in both directions until they extend beyond the field of view. During this stage, the h exhibits an overall increasing trend.

As the VL column cluster becomes unstable and starts to collapse, distinct fluctuations are first observed at the interface of the leftmost VL column at 2.30 s, which subsequently lead to column rupture at 2.60 s. This disturbance then propagates continuously rightward, eventually destabilizing the VL–LL interface of the entire VL column cluster. As a result, the heated wire becomes covered again by a VL film from 2.60 to 3.50 s, accompanied by a subsequent decrease in h. These observations demonstrate a strong coupling between the heat transfer behavior of SFs and interfacial structure evolution. Locally, fluctuations in the h are governed mainly by the spatial density distribution of VL columns. From the viewpoint of heat transfer enhancement, the formation of VL column clusters promotes local recirculation of the cold bulk fluid, thereby intensifying heat exchange between the heated surface and the bulk fluid.

Macroscopically, this phenomenon resembles the minimum heat flux (MHF) point in subcritical boiling.[21] The MHF denotes the minimum heat flux density required to sustain film boiling under subcritical conditions. Nevertheless, the two phenomena differ fundamentally in their microscopic mechanisms because of the essential differences in fluid properties.[22] Under subcritical conditions, interfacial behavior is controlled mainly by buoyancy and surface tension,

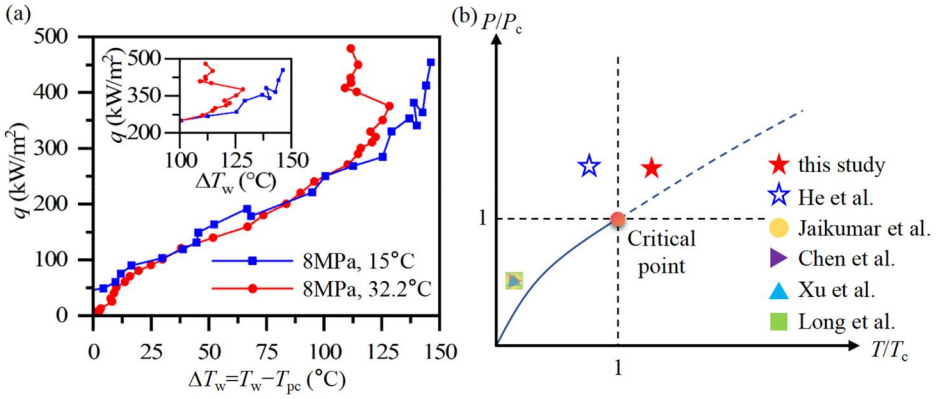


FIG. 1. (a) Heat transfer characteristics of carbon dioxide at 15 and 32.2 °C under a pressure of 8 MPa; (b) summary of previous studies on boiling inversion under different conditions. The wall superheat is defined as $\Delta T_w = T_w - T_{pc}$, with $T_{pc} = 34.67$ °C at 8 MPa.

14 October 2026 07:12:26

Published under an exclusive license by AIP Publishing

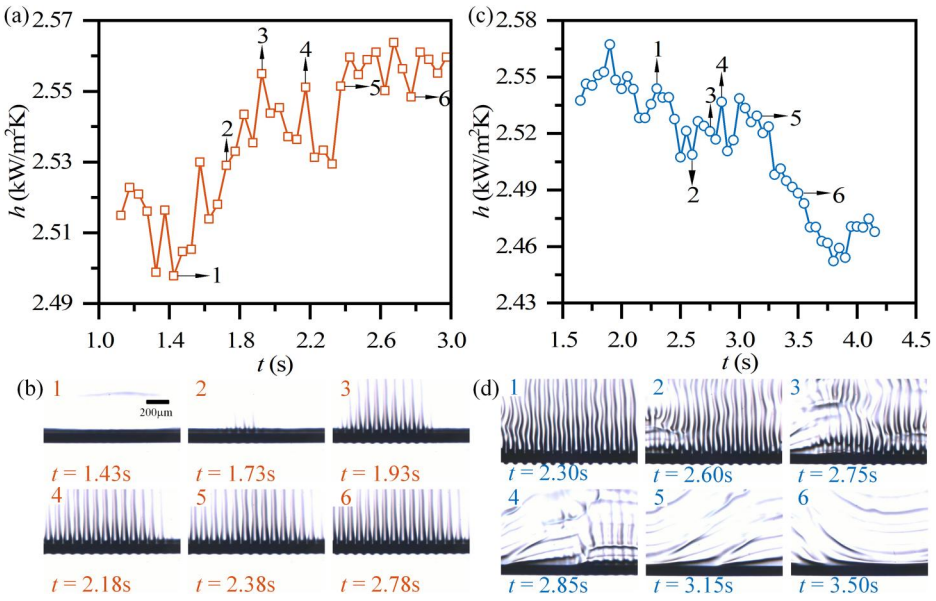


FIG. 2. Formation and collapse of the ordered heat-transfer state. (a) Fluctuations in h during 1.0–3.0 s at $q = 220.24$ kW/m^2; (b) corresponding visualization images during 1.0–3.0 s; (c) fluctuations in h during 1.5–4.5 s at $q = 289.90$ kW/m^2; and (d) corresponding visualization images during 1.5–4.5 s.

and the evolution of interface morphology can generally be interpreted using classical theories such as Rayleigh–Taylor instability (RTI).[23,24] Under supercritical conditions, however, surface tension vanishes,[25] and the interface is no longer subject to capillary restoring forces, fundamentally altering its evolution mechanism. Without such restoring forces, the VL–LL interface becomes highly vulnerable to severe deformation even under weak perturbations, leading to a pronounced reduction in interfacial stability. As a result, the formation of VL column structures becomes less dependent on surface features and more spontaneous. After the VL columns form, the upward transport of the VL fluid and the downward replenishment of the LL fluid generate counterflow-induced shear along the VL–LL interfaces. The resulting interfacial deformation may promote the lateral oscillation and merging of adjacent VL columns, thereby narrowing or locally blocking the LL replenishment pathways. The reduced supply of cold LL fluid causes the fluid retained near the heated wire to be rapidly heated, weakening the local VL–LL density contrast and making the ordered column boundaries difficult to maintain. This process ultimately leads to the nonlinear deformation and collapse of the VL column cluster. These mechanistic differences suggest that interfacial instability in supercritical pseudo-boiling heat transfer should be re-examined, and that new theoretical frameworks applicable to zero surface tension conditions are needed.

The evolution of the VL–LL interface is governed mainly by gravity and buoyancy. Figure 3(a) shows the formation of VL columns and their chain-like diffusion over the entire development process of the VL column cluster. At the initial stage, the heated wire is uniformly covered by a lighter VL film, the VL–LL interface is nearly flat, and a pseudo-phase transition occurs at this interface. Because the heavier fluid overlies the lighter fluid, the system is Rayleigh–Taylor unstable. To further examine this interpretation, a simplified viscous RTI model was used to estimate the characteristic mode of the initial VL–LL interfacial disturbance. The corresponding dispersion relation is $n^2+2\nu k^2 n - Agk = 0$, where n is the growth rate, k is the wavenumber, A is the Atwood number, and ν is the effective kinematic viscosity. Under the representative condition of $P = 8$ MPa, $T_b = 32.2\,^\circ$C, and $T_w = 121.28\,^\circ$C, the predicted fastest-growing wavelength is 138.17 μm, which is close to the measured mean VL column spacing of 95.35 μm. The corresponding characteristic growth time is 2.86 ms, consistent with the millisecond-scale early development observed in the high-speed images (the detailed calculation and comparison are provided in the supplementary material, S3).

Once the interface is perturbed, in the absence of surface tension confinement, the lighter fluid continues to rise under buoyancy, while the heavier fluid moves downward under gravity, leading to separation of the VL and LL flow pathways. In the visualization images, a clear vertical boundary between bright and dark regions is observed above the heated wire. When the cold bulk fluid descends to the hot wall, pseudo-phase transition occurs and converts the heavier fluid into a lighter one. The associated volume expansion drives part of the VL phase downward to form a uniform black bulge beneath the wire, while the remaining part moves upward through the existing VL channels on both sides, appearing as upward growth of these channels. As the newly generated VL phase enters these channels, the flow velocity within the channels increases, and a low-pressure region develops near the channel bottom, which draws in the surrounding stagnant fluid. This process further strengthens the backflow of cold fluid in the LL channels and promotes lateral propagation of the initial disturbance, thereby generating induced disturbances. Under the continued action of RTI, these disturbances are progressively amplified, eventually resulting in the chain-like diffusion of VL columns.

Based on the aforementioned mechanism, the enhanced heat transfer during the formation of VL column clusters arises primarily from the energy release associated with the transition from the VL phase to the LL phase. Because the pseudo-phase transition occurs at the VL–LL interface, and because the temperature differences of the LL phase in the bulk flow and the VL phase surrounding the heated surface can be regarded as approximately constant under specific operating conditions, the heat transfer performance between the wall and the bulk flow can be characterized herein by the total VL–LL

14 October 2026 07:12:26

Published under an exclusive license by AIP Publishing

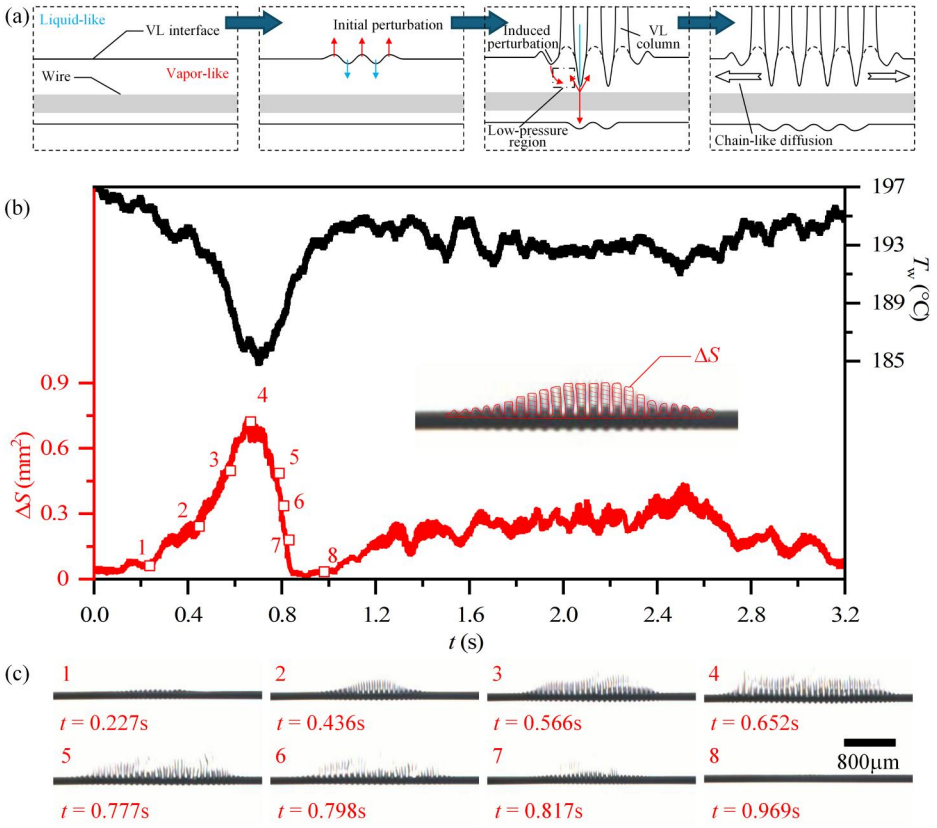


FIG. 3. Chain-like diffusion of vapor-like columns. (a) Schematic of the Rayleigh–Taylor instability induced chain-like diffusion mechanism; (b) fluctuations of the ordered cooling intensity ΔS and wall temperature T_w during 0.0–3.2 s at $q = 289.02$ kW/m^2; (c) corresponding visualization images during 0.0–3.2 s.

interfacial area available for pseudo-phase transition. In the visualization images, this quantity corresponds to the sum of the surface areas of the VL columns and that of the VL film surrounding the wire. To integrate these two contributions, an ordered cooling intensity (S) is introduced and defined as the total area of the VL–LL interface, as shown in Fig. 3(b). Moreover, the corresponding data of ΔS and wall temperature (T_w) over a specific time interval were analyzed, and a strong negative correlation was identified between them (see Fig. S4), indicating that supercritical interfacial phenomena dominate the transient heat transfer process.

The above results indicate that interfacial evolution in SFs plays a decisive role in wall heat transfer, and that the cooling action of the cold bulk fluid on the wall is not continuous but intermittent and governed by hydrodynamic instability. Therefore, clarifying the formation and collapse cycles of VL column clusters is crucial for understanding the overall heat transfer behavior of SFs and for elucidating the mechanism of the inversion of the heat transfer curve. In this respect, this phenomenon plays a role analogous to that of bubble departure frequency in subcritical boiling. Moreover, the formation and diffusion of VL column structures are driven primarily by RTI. For vertically stratified lighter and heavier fluids, the interfacial instability becomes stronger as the density difference increases. At a fixed bulk fluid temperature, this density difference is governed mainly by T_w. Once the T_w exceeds a critical threshold, interfacial phenomena begin to appear and disappear periodically, and the T_w correspondingly exhibits periodic fluctuations due to the periodic sweeping of the wall by the cold bulk fluid. As shown in Fig. 4, at a heat flux of 375.56 kW/m^2, the T_w exhibits low-frequency, high-amplitude oscillations. Combined with the visualization images, it is further found that the fluctuations in T_w are strongly coupled with the interfacial behavior. When interfacial activity occurs (3.3506–3.3806 s), heat transfer is enhanced, and T_w decreases. When it ceases, and the heating wire is again covered by a low-thermal-conductivity VL film (3.3977–3.5058 s), heat transfer weakens, and T_w gradually rises. At this stage, the interfacial behavior no longer shows the regularity and self-similarity observed at lower heat fluxes, but instead exhibits clear chaotic characteristics. This is because, after the T_w increases, the near-wall fluid rapidly absorbs a large amount of heat upon contacting the heated surface, leading to sharp volumetric expansion and strong disturbance of the surrounding flow field. The newly generated VL phase is then governed not only by buoyancy but also by expansion-induced momentum, which drives axial motion. As the fluid expands, the originally uniform black protrusion beneath the wire further develops into a bubble-like structure. The strong axial disturbance makes the VL–LL channel difficult to sustain, so that the VL column clusters tend to collapse as soon as they form, accompanied by substantial heat removal. Therefore, although stable VL column structures are difficult to observe above the wire, the black protrusions beneath the wire (3.3669 s) suggest a common physical origin for the two structures.

Once the wall temperature exceeds a critical threshold, two distinct oscillation modes can be observed simultaneously on the heating wire surface. As shown in Fig. 5, unlike the behavior at lower heat fluxes, the wire in most cases reaches the temperature required to

14 October 2026 07:12:26

Published under an exclusive license by AIP Publishing

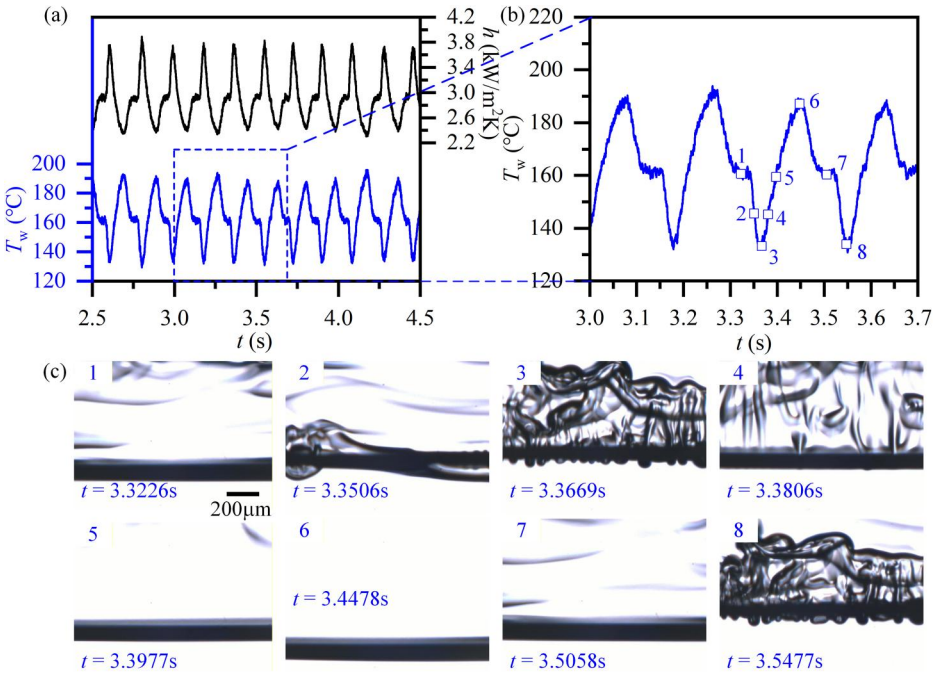


FIG. 4. (a) Fluctuations of T_w and h at $q = 375.56\ \text{kW/m}^2$; (b) enlarged view of T_w fluctuations during 3.0–3.7 s; and (c) corresponding visualization images during 3.0–3.7 s.

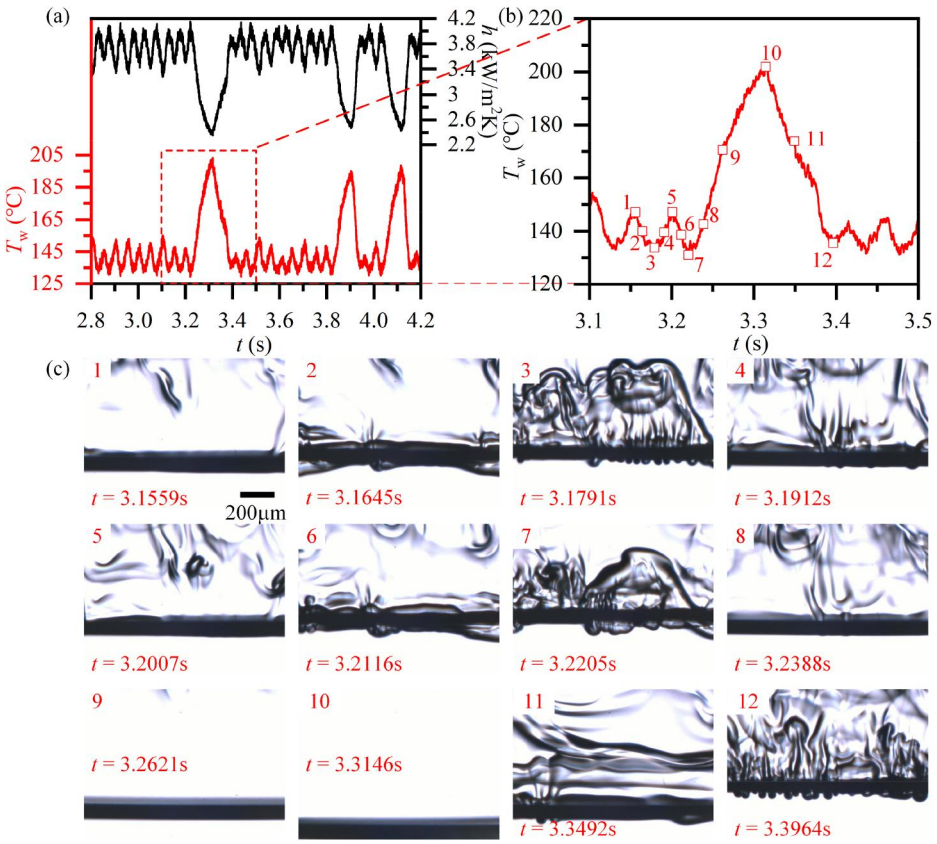


FIG. 5. (a) Fluctuations of T_w and h at $q = 401.25\ \text{kW/m}^2$; (b) enlarged view of T_w fluctuations during 3.1–3.5 s; and (c) corresponding visualization images during 3.1–3.5 s.

14 October 2026 07:12:26

Published under an exclusive license by AIP Publishing

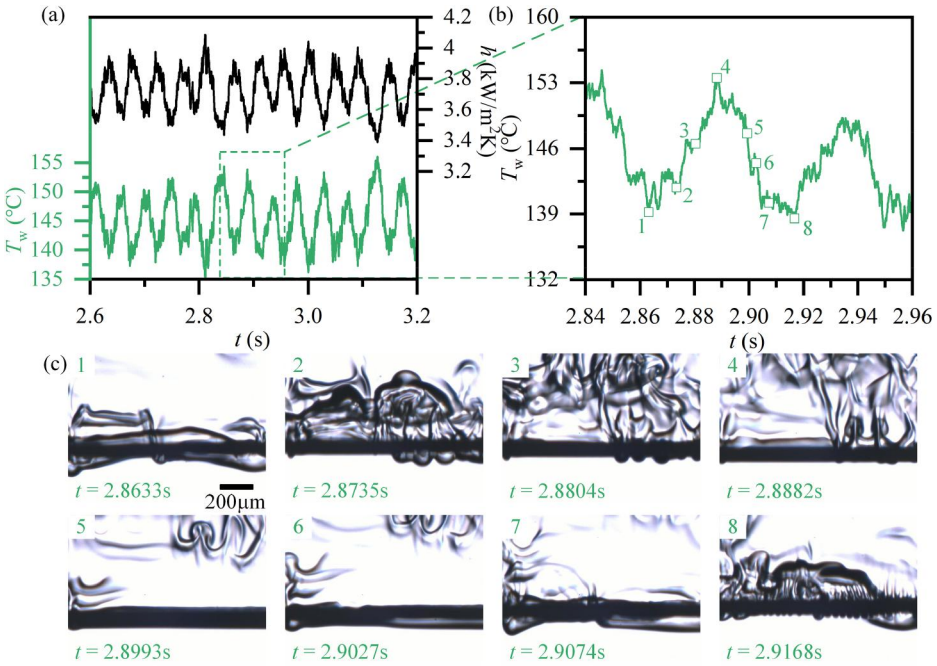


FIG. 6. (a) Fluctuations of T_w and h at $q = 407.94\ \text{kW/m}^2$; (b) enlarged view of T_w fluctuations during 2.84–2.96 s; and (c) corresponding visualization images during 2.84–2.96 s.

trigger interfacial phenomena without a prolonged preparation stage. This indicates that the waiting time for pseudo-boiling nucleation tends to decrease as q increases. Such a trend is similar to that in subcritical boiling, where the bubble cycle shortens with increasing q.[26] When the heat flux reaches 401.25 kW/m^2, the system undergoes a critical transition in its behavior. The T_w then exhibits pronounced multiscale fluctuations, while corresponding interfacial oscillations are simultaneously observed in the visualization images. During 3.2205–3.3964 s, the wire still shows the low-frequency, high-amplitude oscillation mode described above, and pseudo-boiling nucleation is preceded by a relatively long preparation stage (3.2388–3.3146 s). Overall, however, the fluctuations in T_w are dominated by rapid, high-frequency, low-amplitude oscillations. Notably, the T_w remains at a relatively low level throughout this stage, indicating that the sustained occurrence of interfacial phenomena markedly enhances heat transfer and thereby constitutes a decisive factor underlying the reversal of the heat transfer curve.

As q increases further, the T_w fluctuations are completely transformed into a rapid oscillation mode with high frequency and low amplitude (Fig. 6). In this regime, the overall heat transfer performance is markedly enhanced, and the wall superheat decreases further. Analysis of the transient heat transfer data and the synchronized visualization images shows that interfacial activity persists through nearly the entire heat transfer cycle, forming a typical periodic dynamic cycle. Specifically, when the cold bulk fluid contacts the heated surface (2.8633–2.8735 s), pseudo-phase transition is rapidly intensified, as reflected by the continuous expansion of the shadowed region surrounding the wire in the visualization images. Subsequently, once the VL structure detaches from the heated surface and the wall is re-covered by a VL film, the T_w rises rapidly again (2.882–2.899 s) under the high heat flux, and the system enters the next heat transfer cycle.

In summary, using a sCO_2 pool heat transfer system together with transient thermal measurements and synchronized flow visualization, this study clarifies the heat transfer characteristics and interfacial evolution mechanisms of SFs. Inversion of the heat transfer curve is observed within a specific wall-superheat range and is shown to be closely coupled with the periodic formation and collapse of VL column clusters. Further analysis demonstrates that the interfacial evolution is governed mainly by hydrodynamic instability: in the absence of surface tension constraints, the density difference between lighter and heavier fluids drives the chain-like diffusion of VL structures, while shear within the channels induces structural instability. These mechanisms explain the synchronous variations in interfacial behavior and the heat transfer coefficient. On this basis, an *ordered cooling intensity S* is introduced as a unified quantitative parameter to characterize macroscopic interfacial behavior. The significant negative correlation between ΔS and T_w confirms the dominant role of supercritical interfacial phenomena in transient heat transfer. With increasing heat flux, the interfacial-thermal instabilities evolve from low-frequency, high-amplitude fluctuations to rapid oscillations with high frequency and low amplitude. The latter corresponds to the sustained occurrence of interfacial phenomena and is identified as the key mechanism responsible for heat transfer enhancement and reversal of the ΔT_w-q curve.

See the supplementary material for representative studies of boiling inversion; details of the test section, calibration procedure, experimental setup, data reduction, and uncertainty analysis; the relationship between T_w and ΔS; the viscous RTI analysis of the initial VL column formation; and additional experimental results at 12 MPa.

The authors acknowledge the support from the National Natural Science Foundation of China (Nos. 52206197 and 52130608).

14 October 2026 07:12:26

Published under an exclusive license by AIP Publishing

AUTHOR DECLARATIONS

Conflict of Interest

The authors have no conflicts to disclose.

Author Contributions

Guohan Wu: Conceptualization (equal); Data curation (equal); Formal analysis (equal); Funding acquisition (equal); Investigation (equal); Methodology (equal); Resources (equal); Validation (equal); Writing – original draft (lead); Writing – review & editing (lead). **Xiongjiang Yu:** Conceptualization (equal); Data curation (equal); Formal analysis (equal); Funding acquisition (equal); Investigation (equal); Methodology (equal); Resources (equal); Validation (equal); Writing – original draft (lead); Writing – review & editing (lead). **Jinliang Xu:** Conceptualization (equal); Funding acquisition (equal); Resources (equal); Supervision (equal). **Bo Zhang:** Conceptualization (equal); Data curation (equal); Investigation (equal); Supervision (equal); Visualization (equal).

DATA AVAILABILITY

The data that support the findings of this study are available from the corresponding author upon reasonable request.

REFERENCES

[1]Ž. Knez, E. Markočič, M. Leitgeb, M. Primožič, M. K. Hrnčič, and M. Škerget, Energy **77**, 235 (2014).
[2]J. D. Jackson, Nucl. Eng. Des. **264**, 24 (2013).
[3]Z. Y. Liu, L. Chen, and H. Chen, Phys. Fluids **34**, 062003 (2022).
[4]T. Wan, X. J. Wang, Y. X. Jin, and P. H. Zhao, J. Fluid Mech. **1007**, A68 (2025).
[5]G. G. Simeoni, T. Bryk, F. A. Gorelli, M. Krisch, G. Ruocco, M. Santoro, and T. Scopigno, Nat. Phys. **6**, 503 (2010).
[6]J. W. Ackerman, J. Heat Transfer **92**, 490 (1970).
[7]M. Liu, S. Liu, Y. Huang, R. Zheng, H. Yuan, J. Wang, H. Gong, Y. Wang, and S. Huang, Int. J. Heat Mass Transfer **229**, 125669 (2024).
[8]S. Zhang, C. Xiao, D. Gong, and E. Huo, Int. J. Heat Mass Transfer **218**, 124797 (2024).
[9]Q. Wang, X. Ma, J. Xu, M. Li, and Y. Wang, Int. J. Heat Mass Transfer **181**, 121875 (2021).
[10]F. Maxim, K. Karalis, P. Boillat, D. T. Banuti, J. I. Marquez Damian, B. Niceno, and C. Ludwig, Adv. Sci. **8**, 2002312 (2021).
[11]X. He, J. Xu, X. Yu, and J. Xie, Int. J. Heat Mass Transfer **214**, 124417 (2023).
[12]Q. Wang, J. Xu, C. Zhang, B. Hao, and L. Cheng, Heat Transfer Eng. **44**, 1969 (2023).
[13]G. Liang and I. Mudawar, Int. J. Heat Mass Transfer **128**, 892 (2019).
[14]A. Jaikumar and S. G. Kandlikar, in Proceedings of the ASME International Conference on Nanochannels, Microchannels, and Minichannels, 2017.
[15]C. Kruse, A. Tsubaki, C. Zuhlke, T. Anderson, D. Alexander, G. Gogos, and S. Ndao, Appl. Phys. Lett. **108**, 051602 (2016).
[16]A. Jaikumar and S. G. Kandlikar, Appl. Phys. Lett. **108**, 041604 (2016).
[17]A. Jaikumar and S. G. Kandlikar, Appl. Phys. Lett. **110**, 094107 (2017).
[18]R. Chen, M. C. Lu, V. Srinivasan, Z. Wang, H. H. Cho, and A. Majumdar, Nano Lett. **9**, 548 (2009).
[19]J. Xu, W. Ye, X. Yu, and B. Zhang, Nano Lett. **23**, 10021 (2023).
[20]J. Long, Z. Liu, Z. Cao, J. Wu, and X. Xie, Appl. Therm. Eng. **241**, 122330 (2024).
[21]C. Cai, I. Mudawar, and H. Liu, Int. J. Heat Mass Transfer **156**, 119854 (2020).
[22]M. Liu, S. Liu, D. Xi, S. Huang, and Y. Huang, Front. Energy Res. **10**, 1042391 (2023).
[23]H. J. Kull, Phys. Rep. **206**, 197 (1991).
[24]S. D. Park and I. C. Bang, Int. J. Heat Mass Transfer **70**, 844 (2014).
[25]G. L. Weibel and C. K. Ober, Microelectron. Eng. **65**, 145 (2003).
[26]M. Ghazivini, M. Hafez, A. Ratanpara, M. Kim, and J. Therm, Anal. Calorim. **147**, 6035 (2022).

14 October 2026 07:12:26

Published under an exclusive license by AIP Publishing